Geomorphology 216 (2014) 157–170

Contents lists available at ScienceDirect

Geomorphology

journal homepage: www.elsevier.com/locate/geomorph

Avulsion threshold and planform dynamics of the Kosi River in north Bihar (India) and Nepal: A GIS framework

R. Sinha [a,*], K. Sripriyanka [a], Vikrant Jain [b], Malay Mukul [c]

[a] Department of Earth Sciences, Indian Institute of Technology Kanpur, Kanpur 208016, India
[b] Division of Earth Sciences, Indian Institute of Technology Gandhinagar, Ahmedabad 382424, India
[c] Department of Earth Sciences, Indian Institute of Technology Bombay, Mumbai 400076, India

ARTICLE INFO

Article history:
Received 4 January 2013
Received in revised form 19 March 2014
Accepted 24 March 2014
Available online 4 April 2014

Keywords:
Alluvial rivers
Planform dynamics
Avulsion models
Threshold condition
Avulsion prediction
Kosi River

ABSTRACT

Models for river avulsions have identified the ratio between down-valley and cross-valley slopes of channels as the triggering factors for the sudden channel shift but have remained untested in the field. The August 2008 avulsion of the Kosi River at Kusaha, 12 km upstream of the Kosi barrage in Nepal, provided an opportunity to study a large-scale avulsion (~120 km) for its causal factors and driving mechanisms. We used the SRTM-based digital elevation model and remotely sensed data coupled with field topographic mapping with a kinematic GPS and a Total Station to characterise a ~50-km-long stretch of the Kosi River. We have computed reach-scale avulsion threshold index (ATI) integrating SRTM-derived slopes and planform dynamics on a GIS platform. We show that several reaches along the Kosi River are avulsion-prone, including the Kusaha point that is consistent with the August 2008 avulsion. We suggest that apart from cross-valley and down-valley slopes, planform dynamics such as thalweg shift, sinuosity variation, and channel multiplicity significantly influence the avulsion threshold in alluvial reaches of the rivers such as the Kosi.

© 2014 Elsevier B.V. All rights reserved.

1. Introduction

Avulsion has been defined as a rapid and spatially discontinuous shift of a river or a distributary channel to a new course on a lower part of a floodplain (Allen, 1965) and is considered a major fluvial hazard in large population centres (Jain and Sinha, 2004; Sinha, 2009). Avulsion commonly occurs when a reach of the river is at or near an 'avulsion threshold' (Jones and Schumm, 1999) and such shifts in river course significantly influence its morphology, the water and sediment distribution in rivers, and the architecture of fluvial deposits (Törnqvist and Bridge, 2002; Jain and Sinha, 2003; Slingerland and Smith, 2004; Aslan et al., 2005; Stouthamer and Berendsen, 2007). Although avulsions have a strong impact on river morphology and present a major natural hazard, surprisingly little is known about the factors that control avulsion. The avulsion process can be studied through identification and quantitative characterisation of threshold condition(s) and the controlling factors that can help in predicting avulsion (Richards and Clifford, 2011; Jain et al., 2012). The trigger for an avulsion largely depends upon the regional slope conditions and the lowest elevation available in the region. Therefore, topographic analysis is one of the most important components in avulsion studies. In particular, the relationship between the channel slopes in the cross-sectional (cross-valley slope, S_{cv}) and longitudinal direction (down-valley slope, S_{dv}) determines the critical points at which avulsion is likely to occur. A large number of studies on the assessment of avulsion threshold have therefore been based on the examination of longitudinal and cross-sectional morphology of river channels (Bryant et al., 1995; Mackey and Bridge, 1995; Slingerland and Smith, 1998; Ethridge et al., 1999; Mohrig et al., 2000; Karssenberg and Bridge, 2008). Some of these studies have proposed physical and mathematical models for a better understanding of threshold conditions and mechanisms of avulsion and various causal factors, but most of these models have yet to be tested or validated for natural river systems.

Apart from topographic analysis, channel movements and temporal changes in planform characteristics influence the avulsion process. For example, an increase in sinuosity results in the decrease in the down-valley gradient of the channel with respect to cross-valley gradient, which in turn may trigger avulsion (Jones and Schumm, 1999). Changes in channel width and increase in bar area indicate dominance of aggradation processes (Ethridge et al., 1999). Similarly, variation in bar area or braid-channel ratio (Friend and Sinha, 1993) may reflect changes in river behaviour in terms of aggradation and degradation processes, which will have a significant bearing on avulsion process. Therefore, an integration of both morphological and topographic data should provide better insights to avulsion processes.

The Kosi River in eastern India and Nepal has been documented as a highly dynamic river (Geddes, 1960; Gole and Chitale, 1966; Wells and Dorr, 1987; Gohain and Parkash, 1992), and several engineering interventions in terms of a barrage and embankments on both sides of the

* Corresponding author. Tel.: +91 512 6797317; fax: +91 512 679260.
E-mail address: rsinha@iitk.ac.in (R. Sinha).

http://dx.doi.org/10.1016/j.geomorph.2014.03.035
0169-555X/© 2014 Elsevier B.V. All rights reserved.

river during the last 5–6 decades have modified the river processes significantly. One of the serious consequences of these interventions has been a series of breaches in the embankment over the years that often result in large floods. One of the most recent breaches in the eastern embankment occurred at Kusaha in Nepal, 12 km upstream of the Kosi barrage (Fig. 1) on 18 August 2008. This breach resulted in a major avulsion of the Kosi River, which shifted by ~120 km eastward — one of the greatest avulsions in a large river in recent years (Mishra, 2008; Sinha, 2009; Kale, 2011; Sinha et al., 2013). This avulsion resulted in a sheet of flow as wide as ~30 km and inundated a very large area affecting more than 3 million people in Nepal and north Bihar, India. This avulsion occurred at a discharge of 4320 m^3/s (144,000 ft^3/s), which is much lower than the design discharge of 28,500 m^3/s (950,000 ft^3/s) for the barrage and embankments. Using the Kosi avulsion of August 2008 as a case study, this paper aims to test various models for an avulsion threshold and proposes an avulsion threshold index (ATI) that integrates topographic data and planform dynamics.

2. Geomorphic setting and avulsion history of the Kosi River

The Kosi is one of the major tributaries to the Ganga River. Rising in the Nepalese Himalaya, the Kosi River debouches into the plains at Chatra in Nepal and enters India near Bhimnagar. Thereafter, it joins the Ganga River near Kursela, after traversing for ~320 km from Chatra (Fig. 1). The catchment of the Kosi receives a very high rainfall of 1200–2000 mm in most parts (Singh, 1994).

The dynamic nature of the Kosi River has attracted attention for over a century, and a variety of mechanisms have been suggested, ranging from tectonic tilting and nodal avulsions (Geddes, 1960; Gole and Chitale, 1966; Arogyaswamy, 1971; Wells and Dorr, 1987; Agarwal and Bhoj, 1992). The movement of the river has not been gradual but has been avulsive in nature (sudden change in river course) originating from a nodal region (Wells and Dorr, 1987). The published maps show 12 distinct paleochannels of the Kosi, which have been active at different times (Wells and Dorr, 1987; Mishra, 2008; Chakraborty et al., 2010). Chakraborty et al. (2010) revisited the historical-scale migration history of the Kosi and identified three accretionary lobes on the Kosi megafan, although their relative chronology is not clear. An important conclusion of this work was the negation of the idea of continuous westward movement of the river during the pre-embankment period. The authors instead suggested, based on the analysis of historic maps, a random and oscillating shifting of the river except for a prolonged position in the axial part of the river as documented earlier by Gole and Chitale (1966). The average interavulsion period for the Kosi has been recorded as 28 years (Mackey and Bridge, 1995; Stouthamer and Berendsen, 2007), an order of magnitude lower than that of the Mississippi river (~1400 years; Slingerland and Smith, 2004). In a recent work, Sinha et al. (2013) analysed the channel connectivity structure of the Kosi

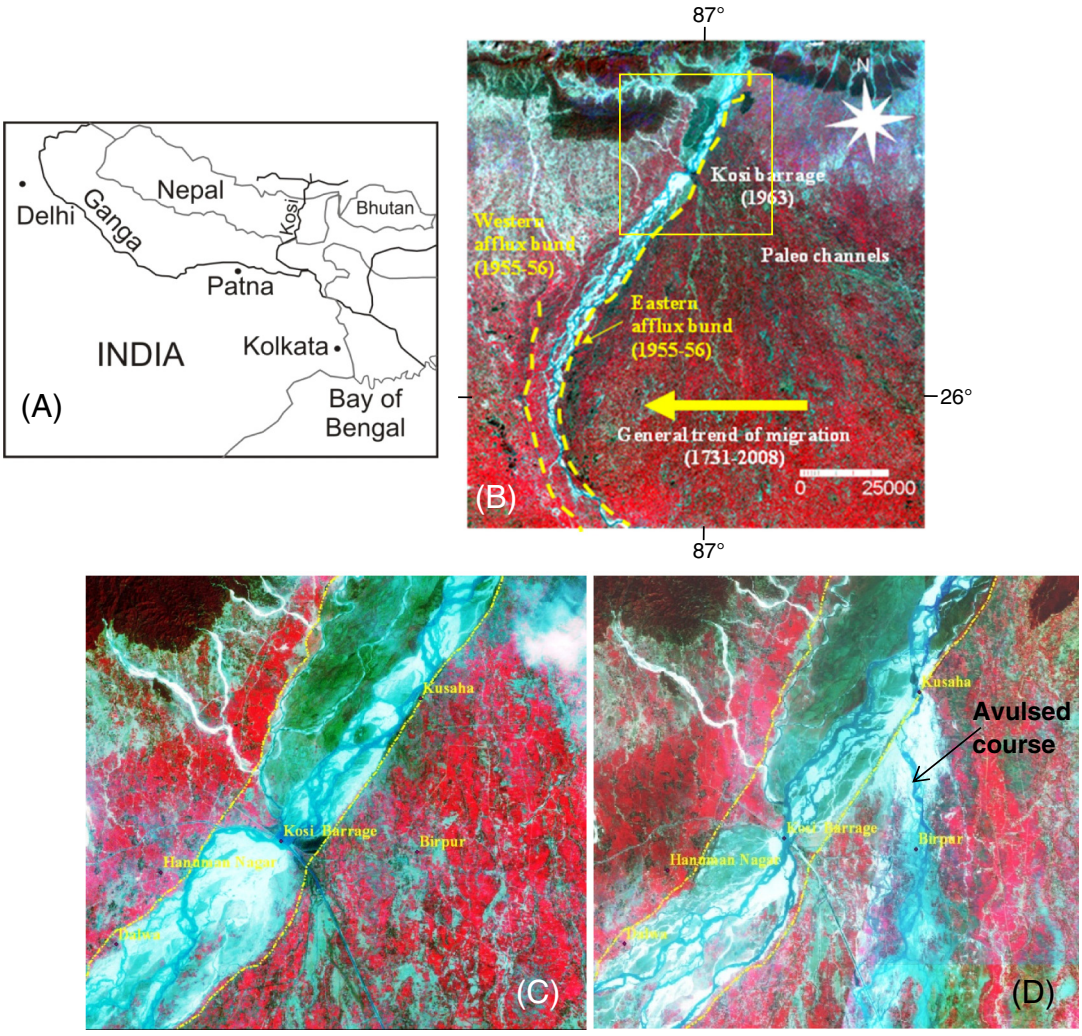

Fig. 1. Location of the study area. (A) Location of the Kosi River in the Indian subcontinent, (B) false colour composite of Landsat image of 2003 showing the Kosi River basin, (C) detailed view of the study area showing the Kosi River during the pre-avulsion period (Landsat image, 2003), (D) detailed view of the study area showing the Kosi River during the post-avulsion period (IRS LISS III image, 2009).

megafan surface and presented a topography-driven model to simulate the avulsion pathway of the August 2008 event.

Early research based on flume experiments and numerical modelling (Mackey and Bridge, 1995) suggested discharge peakedness as one of the causal factors for frequent avulsions and that the avulsion was an autocyclic process in this case. The discharge of the Kosi River varies 5–10 times between the average nonmonsoonal and monsoonal values and this creates channel instability and bank erosion (Sinha and Friend, 1994). An added factor is the high sediment load of the Kosi (43 million tonnes/year) that causes channel bed aggradation. Most of the channel movements of the Kosi also cause extensive flooding, the fan surface being very gently sloping and the channels being shallow.

A major engineering intervention in the form of the Kosi project was commissioned in 1963 that consisted of (i) a barrage at Bhimnagar a few kilometres upstream of the Bihar–Nepal border, and afflux bund; (ii) embankment downstream of the barrage on both sides, 6–7 km apart; and (iii) eastern and western canal system. This project was designed primarily as an irrigation project but was also aimed at restricting the movement of the river and flood protection. However, a total of nine major breaches (Mishra, 2008) accompanied with flooding have occurred between 1963 and 2008 along the eastern as well as the western embankments. In addition, several adverse effects of the Kosi project have been noted such as drainage congestion and water logging, rise of the riverbed level, and reduction in crop productivity due to reduced silt flux onto the floodplains (Mishra, 2008; Sinha et al., 2008; Sinha, 2009). Poor maintenance of the embankments makes the situation even worse.

3. Approach and data

3.1. Models for an avulsion threshold: an overview

One of the early models for an avulsion threshold by Mackey and Bridge (1995) suggested that the location and timing of avulsions are determined by local changes in the floodplain slope relative to the channel belt slope and by the flood magnitude and frequency. The probability of an avulsion for each cross-valley transect (Fig. 2), in case of dependent random avulsion, was computed as,

$$P(a) = \left(\frac{Q_f}{Q_a}\right) e_Q \left(K_s \frac{S_{cv}}{S_{dv}}\right) e_S \quad (1)$$

where Q_f is maximum flood discharge for a given year, Q_a is the threshold discharge necessary for an avulsion, S_{cv} is the cross-valley slope at the edge of the channel belt, S_{dv} is the local down-valley channel-belt slope, K_s is the slope proportionality constant, e_Q and e_S are the avulsion discharge and slope exponents, respectively. Avulsion is triggered when the ratio exceeds unity, i.e. $P(a) \geq 1$.

Bryant et al. (1995) defined a 'superelevated' channel when the sedimentation rates are higher near the channel than farther out in the floodplain (Fig. 2). Under such conditions, avulsion threshold can be defined as

$$\text{Avulsion threshold, } h_e/h > 1 \quad (2)$$

where h_e is the super-elevation of the channel complex above floodplain, and h is the characteristic flow depth (see Fig. 2).

Experimental results generated by Bryant et al. (1995) also showed that the avulsion frequency increased significantly with the increasing sedimentation rate and that the added volume of sediments needed to trigger an avulsion decreased with the increasing sedimentation rate.

Mohrig et al. (2000) interpreted the process of avulsion from the alluvial deposits of the Guadalope–Matarranya system (Oligocene, Ebro basin, Spain) and Wasatch Formation (Eocene, western Colorado, USA) and proposed that the trigger for an avulsion depends upon the levee slope (L_s) and the down-valley slope (S_{dv}) (Fig. 2). The authors suggested that flow depth determines the critical superelevation necessary for channel avulsion. Further, an increase in potential energy owing to aggradation and channel perching increases the instability in lateral channel position and therefore encourages an avulsion. Mohrig et al. (2000) measured geometries of 221 channel fills in the Ebro basin and noted frequent channel reoccupation of the same site by the avulsing channels. It was therefore suggested that the existing paleochannel network on the floodplains provided an important control on the path of the avulsion channels.

The central point in each of the models discussed above is that the 'superelevation' of some part of the channel with respect to the adjoining floodplain provides the 'gradient advantage' for triggering the avulsion and the avulsion channel will follow the locus of maximum floodplain slope. However, given the complexity of the river systems, superelevation defined by individual slope ratios may not be adequate to trigger an avulsion. For example, the levee slope analysis does not consider flow depth as an important parameters even though a channel with a high value for levee slope may not avulse owing to insufficient flow depth. Further, these slope-based indices provide threshold criteria only for static conditions and do not consider temporal changes in

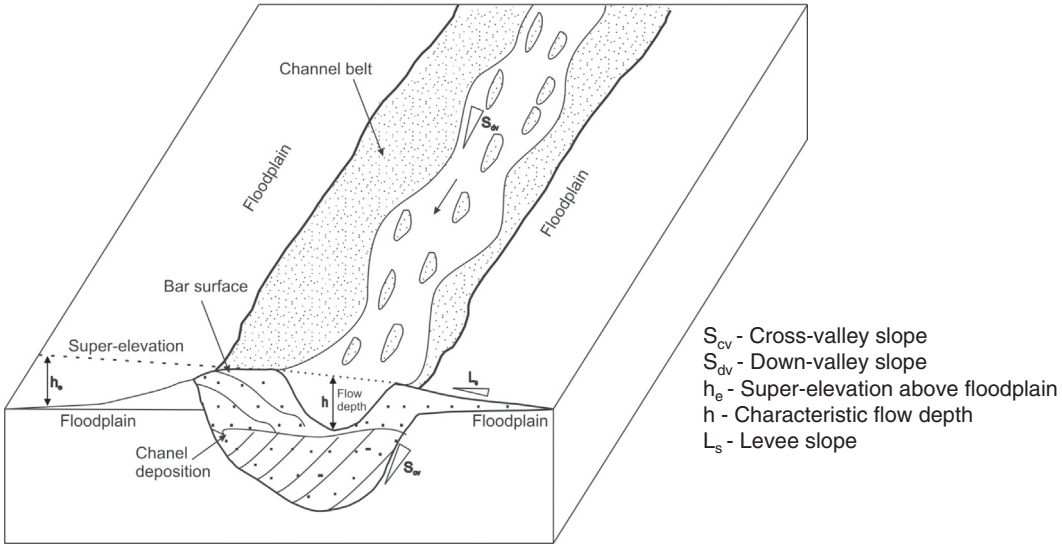

Fig. 2. Conceptual models for avulsion threshold using topographic parameters; Mackey and Bridge (1995) used S_{cv}/S_{dv} ratio; Bryant et al. (1995) used h_e/h ratio, and Mohrig et al. (2000) characterised the super-elevated condition by L_s/S_{dv} ratio.

channel morphology, e.g., the position of main channel (thalweg) within the channel belt and channel processes such as aggradation/degradation.

Keeping in view the limitations of the available avulsion threshold models, this paper integrates all three avulsion threshold models described above with planform dynamics on a GIS platform to propose an avulsion threshold index (ATI). Our study area covers the reaches of the Kosi River upstream and downstream of the Kosi barrage and includes the Kusaha reach in Nepal where the August 2008 avulsion occurred.

3.2. Data used and map analysis

Topographic analysis was carried out with the help of the data from the USGS global digital elevation model (DEM), which has elevation data (SRTM GTOPO30) from the year 2000. A longitudinal profile of the Kosi River was generated for the study window using the spatial profiling tool in Erdas Imagine software. The Kosi channel upstream and downstream of the Kosi barrage was divided into several transects with a spacing of 2 km (Fig. 3), and the down-valley slope (S_{dv}) was calculated for all transects. The Kusaha point falls between transects 6 and 7, and this was analysed separately. Channel cross sections were also generated for every transect, and the plots were smoothed by a 3% running average to remove the noise in the data. The slope between the present channel and the floodplain, termed as the 'cross-valley slope' (S_{cv}), was calculated for every transect and with respect to both embankments. The slope between the embankment (levee) and floodplain, termed as the 'levee slope' (L_s), was calculated for every reach. The difference in elevation between the levee and floodplain was measured to assess superelevation (h_e), and the difference in elevation between levee and channel bed was used to estimate channel depth (h). The ratio between h_e and h was calculated for every reach.

Flow accumulation analysis of the study window was carried out using the SRTM DEM. Flow directions are generally computed using either the MFD (multiple flow direction) model or the SFD (single flow direction) model. Both methods compute downslope flow directions by inspecting the 3-by-3 window around the current cell. The SFD method assigns a unique flow direction toward the steepest downslope neighbour. The MFD method assigns multiple flow directions toward all downslope neighbours. We chose the SFD algorithm because we intend to map the most dominant flow direction along the steepest slope.

Mapping of planform features was carried out with the help of the Landsat 7 ETM image from March 2000 (30-m resolution) and the Indian Remote Sensing satellite (IRS) LISS IV (5-m spatial resolution)

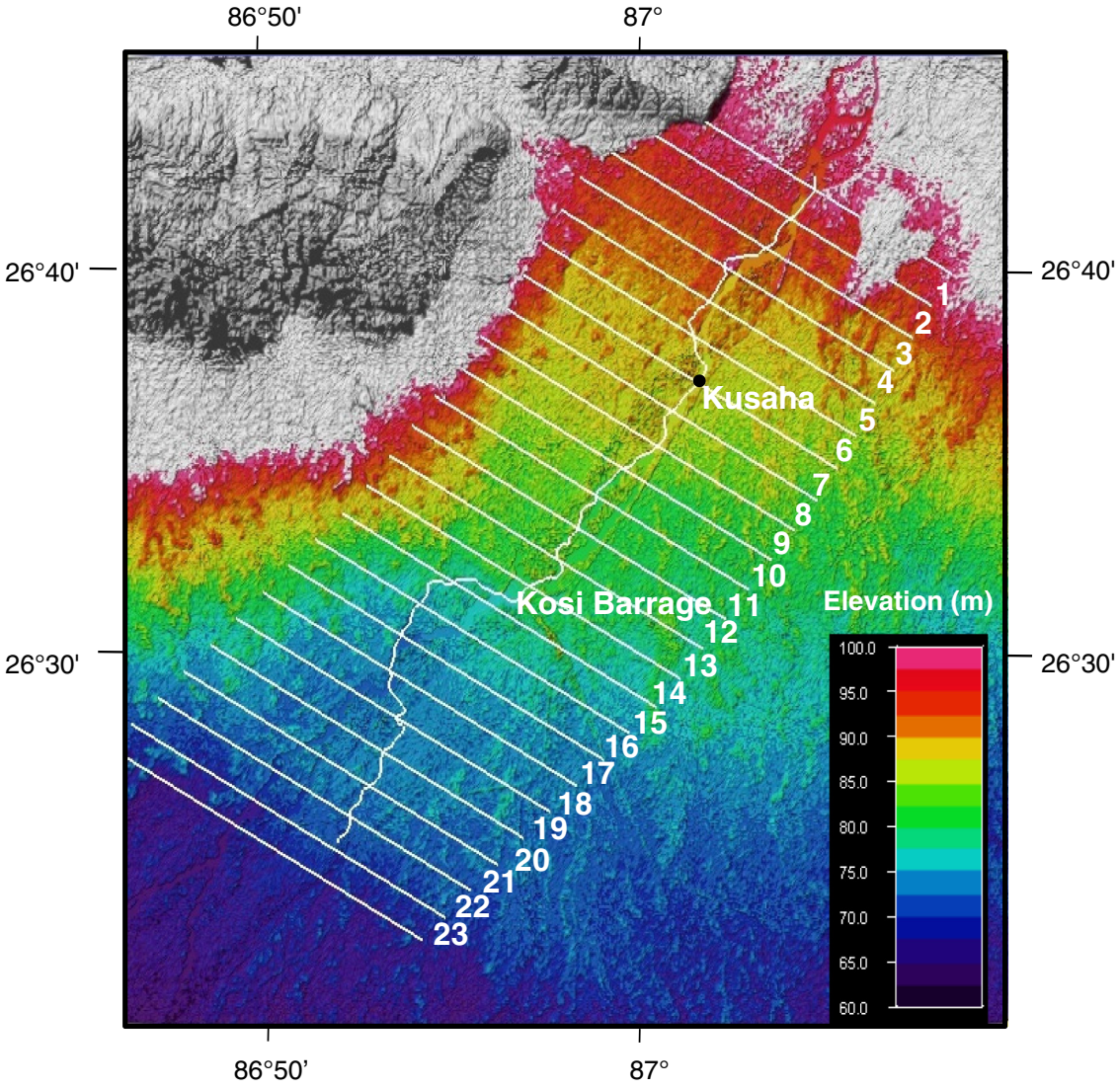

Fig. 3. SRTM DEM showing the thalweg line of the Kosi River and the selected reaches at 2-km-interval. Down-valley slope was computed for each reach and cross sections were taken in the centre of each reach for computing the cross-valley slope. A separate section line at Kusaha (between reaches 6 and 7) was also taken to compute the slope ratios.

images from June 2009. The major avulsion in the Kosi River occurred in August 2008 at the end of the monsoon period. Hence, we presumed that no major planform changes occurred in the Kosi River between August 2008 and June 2009. Georeferencing, visual interpretations as well as digital image processing techniques (such as contrast stretching and image filtering) were applied on the digital data to prepare the geomorphic map, which was also used to analyse planform dynamics. Various planform parameters such as sinuosity and braid-channel ratio (after Friend and Sinha, 1993), channel and channel-belt area, and bar area were estimated from the shape files in the GIS environment. Temporal variations in these parameters were assessed from the measurements from topographic maps and satellite images corresponding to different periods.

3.3. Field surveys

The SRTM-based topographic analyses were further verified through detailed field surveys using the Kinematic GPS and Total Station. The reaches with higher potential of avulsion occurrence on the basis of SRTM-based topographic analysis were selected for field surveys. The Total Station was used in prism mode with ±2-mm measurement accuracy. The Kinematic GPS was used to prepare the channel cross sections along transect lines, while Total Station based surveys were carried out to analyse surface elevation on either side of the western embankment. A total of three cross-sectional profiles were surveyed across the western embankment.

The Kinematic GPS surveys were carried out along three transects (4, 7, and 11) across the Kosi River channel (Fig. 3). One transect (11) was located immediately upstream of the Kosi Barrage and the other two transects (4 and 7) were chosen north and south of Kusaha. The survey involved the use of two dual frequency Trimble R5 receivers in Real Time Kinematic mode and an operational accuracy ranging from ±5 to ±10 cm.

3.4. Analytical hierarchy process (AHP) analysis

We have integrated the different geomorphic drivers of avulsion as discussed above in a GIS environment using one of the multicriteria techniques called 'analytical hierarchical process' (AHP), which is based on a 9-point scale (Saaty, 1980; Siddique et al., 1996). This method involves a pairwise comparison of the relative preferences of the different drivers, called 'decision factors', for avulsion threshold assessment after constructing a 'decision hierarchy'. The first level of the hierarchy represents the goal, while the rest of the levels describe the factors and subfactors in increasing details. This was followed by estimation of Eigen vectors by multiplying all the elements in a row and taking the *n*th root of the product, where n is the number of row elements. The next step involves the determination of relative importance weight (RIW) for each hierarchy element by normalizing the Eigen vector of the decision matrix (Saaty, 1980). Normalization of the Eigen vectors was done by dividing each Eigen vector element by the sum of all Eigen vector elements in a particular matrix. Finally, an avulsion threshold index (ATI) was computed using the equation

$$\mathrm{ATI} = \sum_{i=1}^{N_2} \left[\left(\mathrm{RIW}_i^2 \right) * \left(\mathrm{RIW}_{ij}^3 \right) \right] \quad (3)$$

where N_2 is the number of level 2 decision factors, RIW_i^2RIW is the relative importance weight of level 2 decision factor *i*, and RIW_{ij}^3RIW is the relative importance weight of level 3 subfactor *j* of level 2 decision factor *i*.

The AHP is a very flexible and powerful tool for multicriteria complex decision making as it helps to capture both subjective and objective aspects of a decision through a series of pairwise comparisons. This method provides an opportunity to consider a set of evaluation criteria and set of alternative options among which the best decision can be made.

4. Results and analysis

4.1. Flow accumulation analysis

A flow accumulation map of the study area was generated from the SRTM data (Fig. 4) that represents the natural flow direction for every pixel in the DEM. Flow lines within the embankments have shades of grey and somewhat white colour suggesting multichannel flow typical of a braided system. A strong flow accumulation path around Kusaha flows outside the embankment and continues for several kilometres downstream of Birpur. It suggests that the normal flow direction around the avulsion site at Kusaha is toward the southeast (outside the embankment). Field observations suggest that this represents a well-defined seepage channel originating off the embankment around Kusaha and then joining one of the paleochannels downstream (Fig. 5A). A major proportion of the flow during the August 2008 avulsion passed through this channel, and this remains an active channel after the avulsion (Fig. 5B).

4.2. Cross-sectional morphology and slope ratios

Cross sections were generated from the SRTM data for different reaches extending from the channel belt to floodplains on either side. Two distinct types are identified: one is the 'normal' cross section in which the floodplain is at a higher elevation than the channel (Fig. 6A) and the other is the 'super-elevated' cross section where the channel is at higher elevation than the surrounding floodplain as shown in Fig. 6B. Using the cross sections, the cross-valley slope (S_{cv}), levee slope (L_s), superelevation channel complex height above the floodplain (h_e), and characteristic flow depth (h) were calculated with reference to the eastern embankment (see Fig. 2). The cross-valley slope (S_{cv}) toward the channel was considered as negative and the same away from the channel (super-elevated condition) was considered as positive. Similarly, the down-valley slope (S_{dv}) was calculated for every 2-km-long reach from the SRTM-derived longitudinal profile. A separate cross section was taken at the Kusaha point. Using these measurements, the ratios S_{cv}/S_{dv}, Ls/S_{dv}, and h_e/h were computed — which have been defined as avulsion thresholds by different workers (Bryant et al., 1995; Mackey and Bridge, 1995; Mohrig et al., 2000).

Fig. 7 shows a plot of all three ratios for the different reaches. While the actual values of these ratios are different, they follow a similar trend. Several reaches show high values of these ratios, suggesting a higher probability of avulsion at these points. These data have been further integrated with data on planform dynamics to compute the ATI.

4.3. Planform dynamics

Fig. 8 shows a noticeable decrease in sinuosity in a few reaches (such as 2, 4, 14 and 19) between 1983 and 2000. However, the changes in braid-channel ratio are much more remarkable. Almost all reaches upstream of the barrage show a decrease in braid-channel ratio (after Friend and Sinha, 1993), e.g., from 12.7 to 3.8 between 1983 and 2000 in reach 3. Downstream of the barrage, the first four reaches show a decrease in braid-channel ratio from values around 4.5–5.0 to 3.0, but the remaining reaches show an increase. Further, bar area shows a two-fold increase in the reaches upstream of the barrage (Fig. 9A) and a three-fold increase in the reaches downstream of the barrage. This is a manifestation of a much reduced capacity of the channel to transport sediments caused by velocity reduction and slope changes induced by barrage construction. Upstream of the barrage, temporary storage of water results in settling of sediments, whereas channel widening in the reaches downstream of the barrage (except for the reaches adjacent

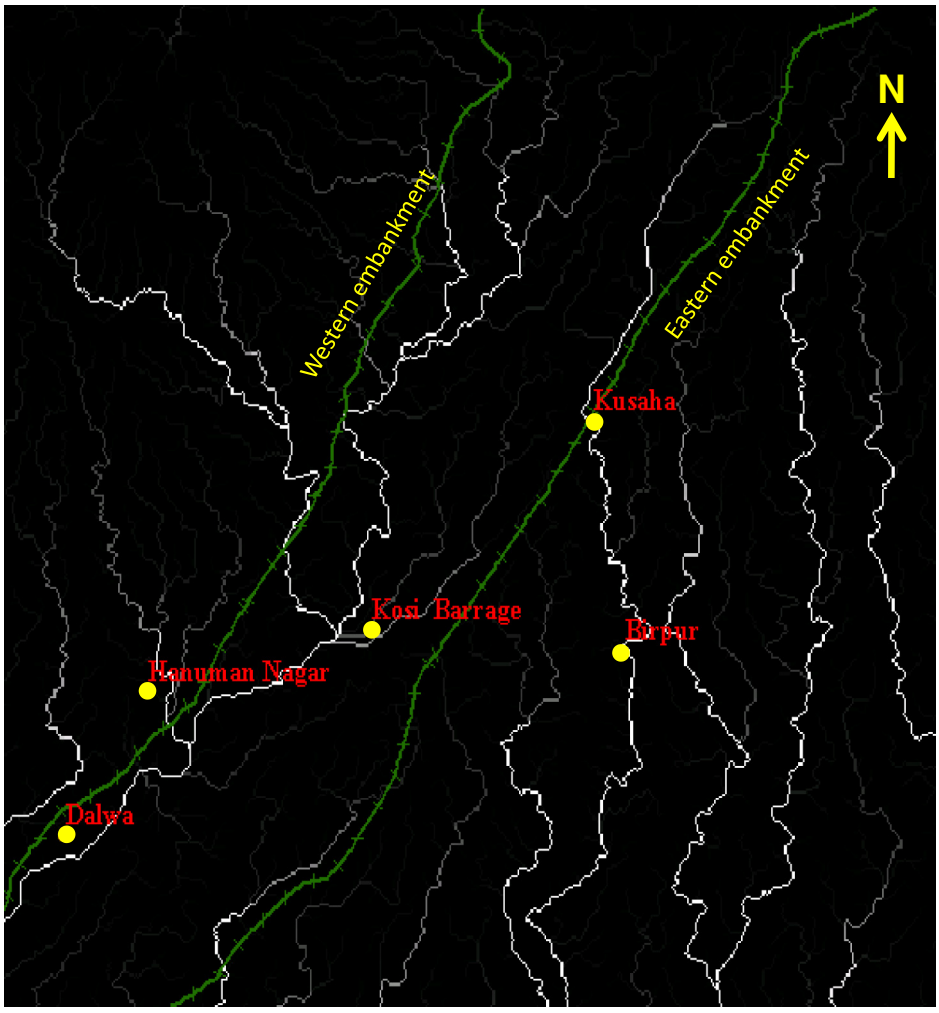

Fig. 4. Flow accumulation map of the study area based on the SRTM data of the year 2000 using single flow direction (SFD) algorithm. A prominent flow line across the embankment (in green) around Kusaha is noticeable. (For interpretation of the references to colour in this figure legend, the reader is referred to the web version of this article.)

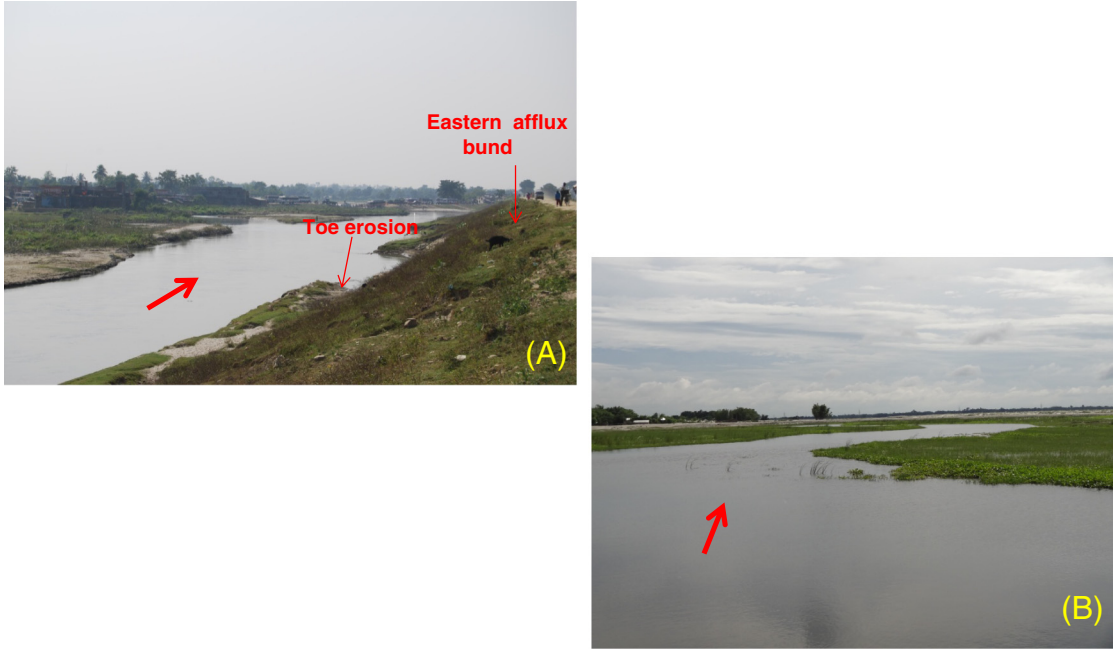

Fig. 5. (A) A seepage channel close to Kusaha as observed in October 2008 after the avulsion; the channel was more than 20 m wide and the maximum water depth was ~1 m; (B) field view of the same seepage channel at Birpur, 12 km downstream of Kusaha as observed in September 2012; a clear expansion of flow was observed as the channel widened to more than 100 m.

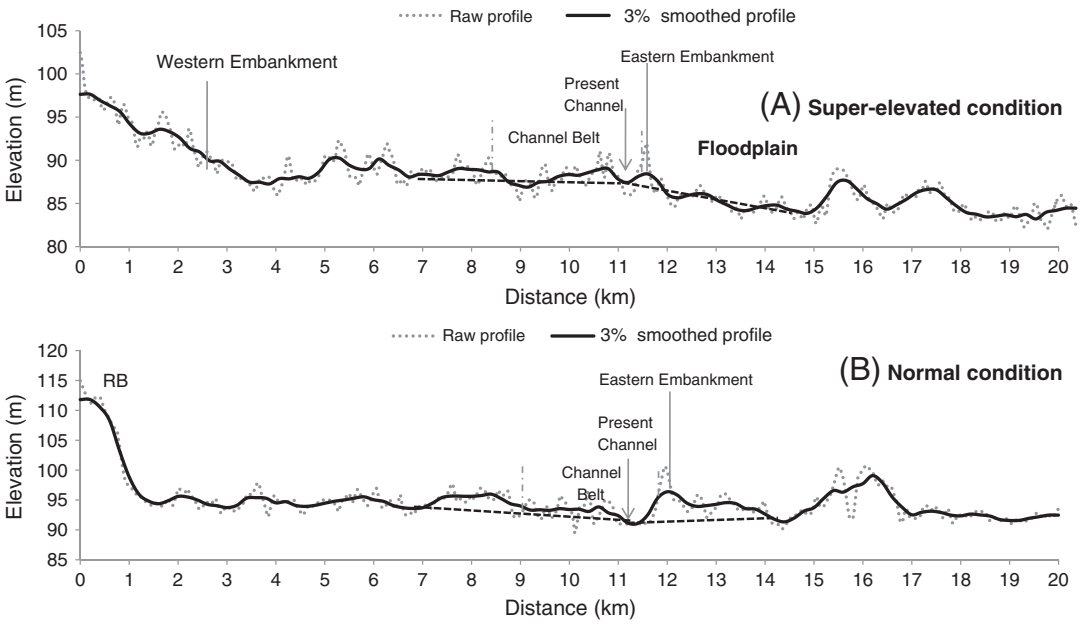

Fig. 6. Cross-sectional profiles for (A) reach 7 (close to Kusaha) representing the super-elevated condition and (B) reach 2 (upstream of Kusaha) representing the normal condition.

to the barrage that are protected) results in reduced flow depth and sedimentation. However, channel area shows a mixed trend (Fig. 9B); it decreased drastically (by ~88%) in the reaches upstream of the barrage, but no clear trend is observed in the reaches downstream of the barrage. This is related to the barrage operation policy and is primarily controlled by the opening of gates at different times. Changes in channel-belt area (Fig. 9C) nearly mimic those in bar area suggesting a greater influence of sedimentation than that of erosion.

The period from 2000 to 2009 shows different scenarios (Figs. 8,9). Sinuosity values remained almost the same in most of the reaches. Braid-channel ratio decreased significantly in reaches 4 and 8, while it increased in reaches downstream of the barrage. Further, most of the reaches are characterised by an increase in bar and channel-belt areas, which suggests extensive aggradation in these reaches during this period. Channel area shows a variable trend, but decreased in reaches 1–17 and increased in reaches 18–23 with respect to 1989.

The movement of the thalweg of the main channel with reference to the western and eastern embankments for the period 1983–2009 is shown in Fig. 10. The thalweg in 1983 was very close to the western embankment in most parts of the study reach. The maximum shift in the thalweg is measured as 7.2 km (eastward) in reach 8 during the period 1983–2000, while reach 19 is the most stable with almost no shift at all. The 2000 thalweg is very close to the eastern embankment in the reaches upstream of the barrage and then swings toward the western embankment. The thalweg in 2009 (post-avulsion) is fairly central, and the maximum shift in the thalweg is measured as 3.8 km

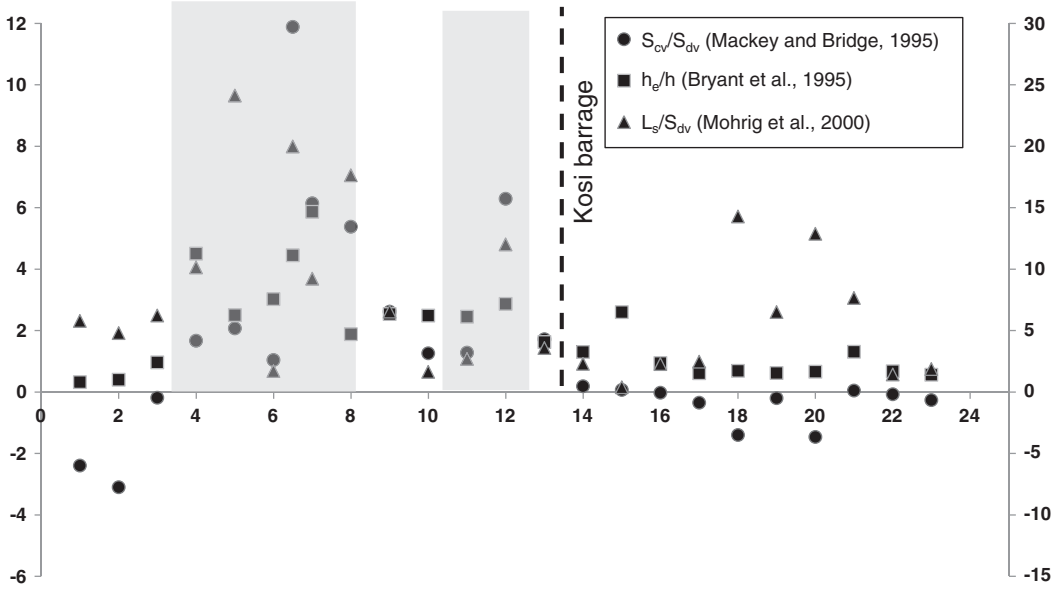

Fig. 7. Reaches marked in grey boxes show high values (≫1) for all three ratios.
Slope ratios for different reaches as defined by Bryant et al. (1995), Mackey and Bridge (1995), and Mohrig et al. (2000).

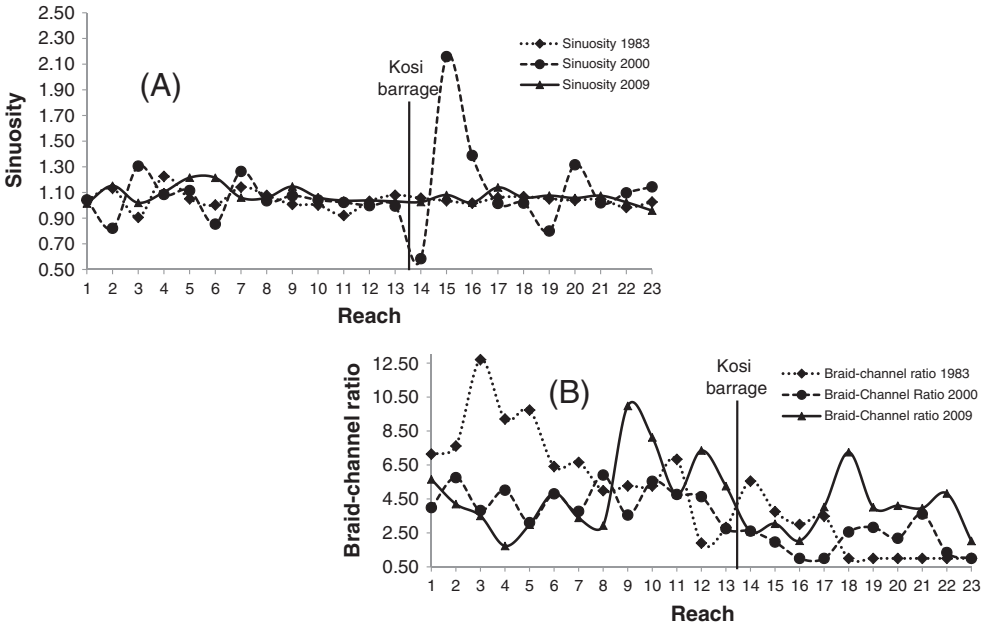

Fig. 8. Reach wise plot of (A) sinuosity and (B) braid-channel ratio for the years 1983, 2000 and 2009. Sinuosity values decreased through time in most reaches, whereas the braid-channel ratio decreased in reaches upstream of the barrage but increased in several downstream reaches.

(eastward) in reach 17, while reach 1 is the most stable with a shift of only 711 m (westward) during the period 2000–2008.

4.4. Data integration in GIS environment using analytical hierarchy process (AHP)

Tables 1 and 2 show the decision hierarchy built for avulsion threshold analysis. Amongst the two sets of criteria viz. slope ratios and planform dynamics, the former has been put at a higher level of hierarchy owing to the dominant control of slope on avulsion. Among the slope factors for the avulsion threshold, we have decided the hierarchy as follows:

- The S_{cv}/S_{dv} is considered as the most important factor for triggering the avulsion as it is the first indicator of channel super-elevation with respect to floodplain.

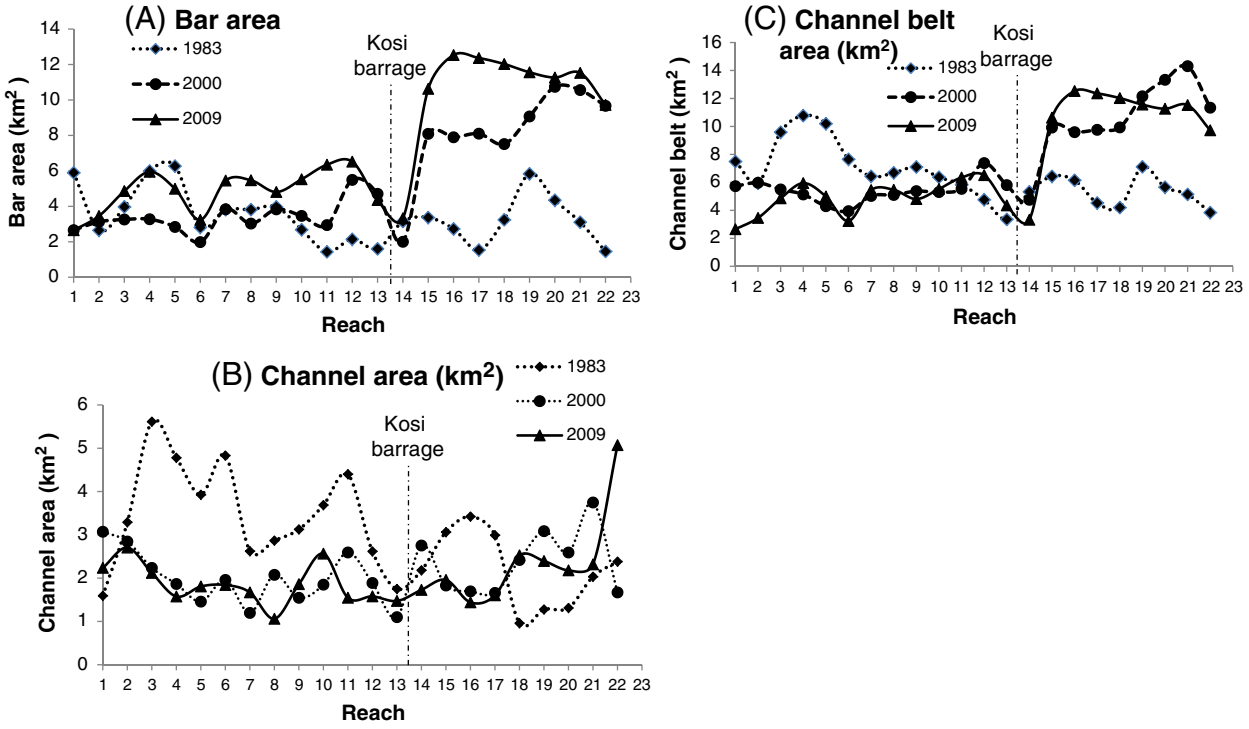

Fig. 9. Reachwise plot of (A) bar area, (B) channel belt area and (C) channel area for the years 1983, 2000, and 2009. Channel area shows a mixed trend but the bar area shows an increase in most reaches upstream and excessive aggradation downstream. Channel belt shows a distinct decrease in the reaches downstream of the barrage suggesting channel expansion.

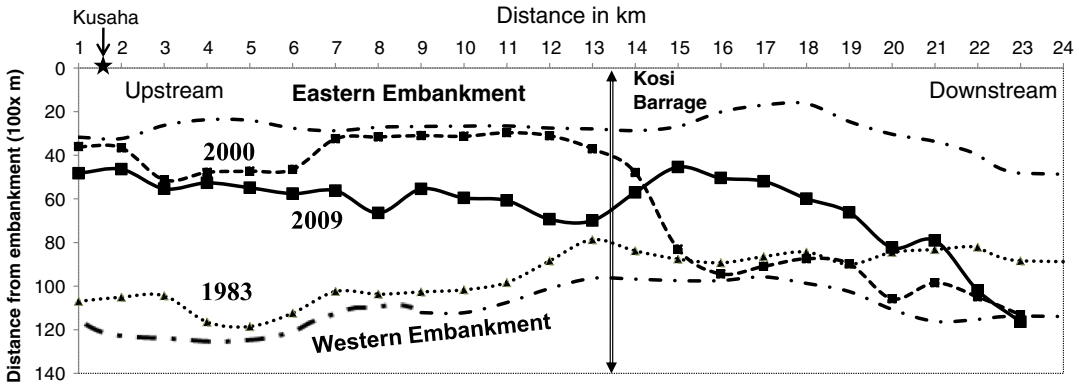

Fig. 10. Map showing the positions of channel thalweg with respect to the eastern and western embankments for the years 1983, 2000 and 2009. Location of the breach point at Kusaha during the August 2008 avulsion is also shown. Noticeably, the channel thalweg was very close to the embankment around the Kusaha point since 2000.

- The second important factor is super-elevation to flow depth (h_e/h) because it is determined by channel position, super-elevated scenario, and the levee height.

The super-elevation of the channel with respect to the floodplain is also determined by L_s/S_{dv} but less directly, and therefore we have put this at a slightly lower hierarchy. While these topographic indices will provide quantitative information about avulsion potential, the likelihood of an avulsion event at any reach will be finally governed by the position of channel with respect to embankment (will also provide the maximum cross-valley slope) and planform dynamics over time. Therefore, channel position with respect to embankment and parameters related to planform dynamics were kept at the next level of hierarchy after topographic indices. Among the planform parameters, we have considered bar area ratio, channel area ratio, channel-belt area ratio, braid-channel ratio, and sinuosity in the order of hierarchy.

To maintain uniformity with the slope data derived from SRTM data of the year 2000, we have used the planform variability between 2000 and 2009 for the avulsion threshold analysis using AHP. Channel position was defined for the year 2000 (pre-avulsion period) to maintain conformity with the SRTM data. Bar area ratio is a manifestation of channel aggradation and is responsible for pushing the channel to a super-elevated condition. Channel area ratio is complementary to the effect of bar area increase under natural conditions. Channel belt area ratio integrates the effect of channel and bar area ratios on the channel with reference to avulsion. Braid-channel ratio is considered as an important parameter because variations in bar area ratio are reflected in variations of braid-channel ratio. Finally, sinuosity is considered as one of the decision factors; although it does not play a major role in triggering the avulsion but often pushes the river toward avulsion threshold.

Based on the histogram (Fig. 11), the ATI values thus obtained for different reaches of the Kosi River were classified (Table 3).

Reaches 4, 5, 7 and 8 show ATI values of >0.35 ($\mu + \sigma$), similar to Kusaha, and we have designated these reaches as 'most critical'. This is an important observation that suggests that the river was close to avulsion threshold from the year 2000 itself but continued to flow within the embankments. By the year 2008, the river crossed the threshold, breached the eastern embankment, and avulsed to a new course. Further, six reaches (6, 9, 10, 11, 12, and 13) show ATI values greater than the average (0.25) but less than the critical value (0.35), and we consider these reaches to be 'critical' (Fig. 11). The remaining reaches which have ATI values less than the average are considered as less vulnerable to avulsion. Two of the 'most critical' reaches (4 and 7) and one of the critical reaches (11) were further analysed through high resolution field survey (discussed next).

4.5. Field validation using high resolution topographic surveys

High resolution topographic survey data for a few selected (most critical) reaches using Kinematic GPS and Total Station were used to validate the avulsion threshold analysis. Fig. 12 shows the profiles across the channel (4, 7 and 11; see Fig. 3 for location) based on kinematic GPS surveys. Elevation of bar surface within the embankment area was considered to represent channel bed surface during flood, and the surface outside the embankment is defined by the floodplain. Further, the analysis was carried out by considering other geomorphic

Table 1
Pairwise comparison matrix for level 2 decision factors.[a]

Decision factors	S_{cv}/S_{dv}	h_e/h	L_s/S_{dv}	Channel position	Bar area	Channel area	Channel belt area	Braiding index	Sinuosity	EEE	RIW
S_{cv}/S_{dv}	1	2	2	3	4	5	6	7	9	3.56	0.250
h_e/h	1/2	1	2	3	5	5	6	7	9	3.12	0.220
L_s/S_{dv}	1/2	1/2	1	3	5	5	6	7	9	2.68	0.188
Channel position	1/3	1/3	1/3	1	4	6	7	8	9	1.97	0.138
Bar area	1/4	1/5	1/5	1/4	1	6	7	8	9	1.25	0.088
Channel area	1/5	1/5	1/5	1/6	1/6	1	7	8	9	0.78	0.055
Channel belt area	1/6	1/6	1/6	1/7	1/7	1/7	1	8	9	0.46	0.033
Braiding index	1/7	1/7	1/7	1/8	1/8	1/8	1/8	1	8	0.26	0.018
Sinuosity	1/9	1/9	1/9	1/9	1/9	1/9	1/9	1/8	1	0.14	0.010

[a] This table is an $m \times m$ real matrix, where m is the number of evaluation criteria considered. Each entry a_{jk} of the matrix represents the importance of the jth criterion relative to the kth criterion using the 9-point scale of Saaty (1980) as follows: 1 — both factors are equally important; 3 — weak importance of one over the other; 5 — essential or strong importance; 7 — demonstrated importance; 9 — absolute importance; 2,4,6,8 — intermediate values between two adjacent judgments. If $a_{jk} > 1$, then the jth criterion is more important than the kth criterion; while if $a_{jk} < 1$, then the jth criterion is less important than the kth criterion. If two criteria have the same importance, then the entry a_{jk} is 1. The entries a_{jk} and a_{kj} satisfy the following constraint: $a_{jk} * a_{kj} = 1$. Obviously, $a_{jj} = 1$ for all j (EEE = estimated eigen element; RIW = relative importance weightage).

Table 2
Calculation of relative importance weightage for level 3 subfactors.

S_{cv}/S_{dv}	>3	1.5–3	0–1.5	<0	EEE	RIW	L_s/S_{dv}	>15	10–15	5–10	<5	EEE	RIW
>3	1	2	3	6			>15	1	2	3	6	2.45	0.46
1.5–3	1/2	1	3	6	1.73	0.32	10–15	1/2	1	3	6	1.73	0.32
0–1.5	1/3	1/3	1	6	0.90	0.17	5–10	1/3	1/3	1	6	0.90	0.17
<0	1/6	1/6	1/6	1	0.26	0.05	<5	1/6	1/6	1/6	1	0.26	0.05
h_e/h	>3.5	1.5–3.5	1–1.5	<1	EEE	RIW	Bar area ratio	>8	3–8	0.46–3	<0.46	EEE	RIW
>3.5	1	2	3	6			>8	1	3	5	7	3.20	0.54
1.5–3.5	1/2	1	3	6	1.73	0.32	3–8	1/3	1	5	7	1.85	0.31
1–1.5	1/3	1/3	1	6	0.90	0.17	0.46–3	1/5	1/5	1	3	0.59	0.10
<1	1/6	1/6	1/6	1	0.26	0.05	<0.46	1/7	1/7	1/3	1	0.29	0.05
Channel area ratio	<0.4	0.4–0.5	0.5–2.5	>2.5	EEE	RIW	Channel belt area ratio	<0.43	0.43–1	1–2.8	>2.8	EEE	RIW
<0.4	1	3	5	7	3.20	0.54	<0.43	1	2	3	4	2.21	0.45
0.4–0.5	1/3	1	5	7	1.85	0.31	0.43–1	1/2	1	3	4	1.57	0.32
0.5–2.5	1/5	1/5	1	3	0.59	0.10	1–2.8	1/3	1/3	1	4	0.82	0.16
>2.5	1/7	1/7	1/3	1	0.29	0.05	>2.8	1/4	1/4	1/4	1	0.35	0.07
Braid-channel ratio	>3.5	1–3.5	0.16–1	<0.16	EEE	RIW	Sinuosity ratio	>2	1–2	0.6–1	<0.6	EEE	RIW
>3.5	1	2	5	7	2.89	0.50	>2	1	2	5	7	2.89	0.50
1–3.5	1/2	1	5	7	2.05	0.35	1–2	1/2	1	5	7	2.05	0.35
0.16–1	1/5	1/5	1	3	0.59	0.10	0.6–1	1/5	1/5	1	3	0.59	0.10
<0.16	1/7	1/7	1/3	1	0.29	0.05	<0.6	1/7	1/7	1/3	1	0.29	0.05

Channel position (km)	<2	2–5	>5	EEE	RIW
<2	1	3	7	2.76	0.63
2–5	1/3	1	7	1.33	0.30
>5	1/7	1/7	1	0.27	0.06

surfaces, namely main channel, surface between the guide bunds (embankment to guide the channel), and a seepage channel close to the embankment.

The geomorphic condition of these reaches was further assessed by computing elevation difference between different surfaces across the embankment, super-elevation condition (SC), cross-valley slope (S_{cv})

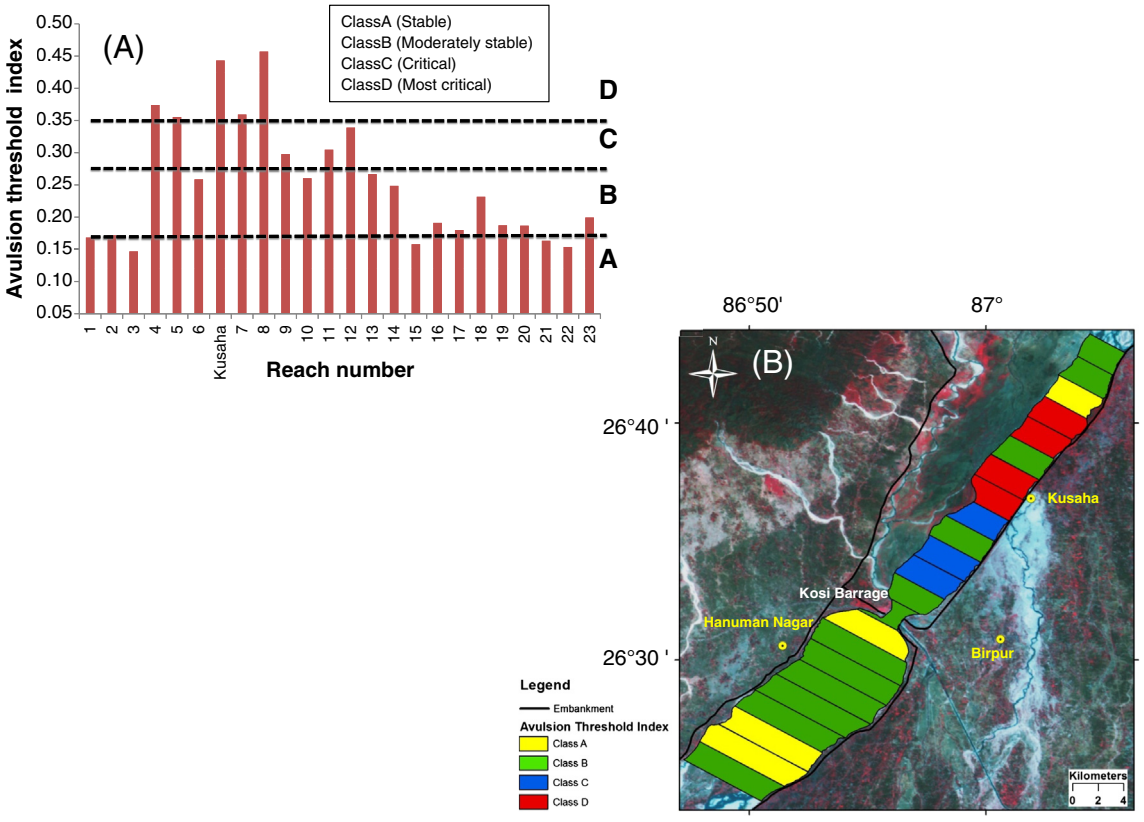

Fig. 11. (A) Avulsion threshold index (ATI) values of different reaches after AHP analysis and their categorization into four classes (A, B, C, and D) where D is the most critical class. (B) Avulsion threshold index (ATI) plotted for the reaches of the Kosi River upstream and downstream of the barrage. Several reaches upstream of the barrage, including the Kusaha point, are classified as 'most critical' and 'critical'. Most reaches downstream of the barrage are stable to moderately stable.

Table 3
Classification of ATI values[a].

Class	Criteria	ATI value	Designation
Class A	ATI ≤ ($\mu - \sigma$)	≤0.16	Stable
Class B	($\mu - \sigma$) < ATI ≤ μ	0.16 < ATI ≤ 0.25	Moderately stable
Class C	μ < ATI ≤ ($\mu + \sigma$)	0.25 < ATI ≤ 0.35	Critical
Class D	ATI > ($\mu + \sigma$)	>0.35	Most critical

[a] μ = mean of ATI (=0.25); σ = standard deviation of ATI (=0.09).

and down-valley slope (S_{dv}) across these cross sections (Table 4). In all three cross sections, the bar surface is ~2 m higher than the floodplain surface. The presence of a seepage channel increases this difference further to ~4 m and makes the site more prone for avulsion process. The super-elevation in these cross sections on the basis of bar-floodplain surfaces varies from 1.55 to 1.75 m and for bar-seepage channel surfaces from 1.89 to 2.61 m. Even for other surfaces across the embankment, the super-elevation remains more than 1. A comparison of down-valley slope (S_{dv}) and cross-valley slope (S_{cv}) reveals that S_{cv} is significantly higher than S_{dv} at all the cross sections; and therefore, these cross sections are highly vulnerable to avulsion as demonstrated earlier.

These cross sections measured by Kinematic GPS define the elevation variation along a transect line only. To validate our results further, detailed surface analysis was carried out using Total Station at Kusaha and downstream. Total Station data (Fig. 13) also show a similar pattern and confirm the super-elevated condition at this site. In general, the bar surface toward the eastern embankment is 2–3 m higher than the floodplain surface. Our high resolution detailed topographic survey supports the topographic analysis on the basis of SRTM data. The 'most critical' reaches on the basis of SRTM data are also defined as high potential avulsion sites on the high resolution topographic data.

5. Discussion

5.1. Avulsion threshold indices — comparison of different approaches

Fig. 7 shows the avulsion threshold indices computed by using the criteria defined by Bryant et al. (1995), Mackey and Bridge (1995), and Mohrig et al. (2000). Notably, the results from three different approaches do not match completely. However, several reaches (e.g. 4, 5 Kusaha, and 8) show high values for all three methods suggesting higher probability of avulsion, and this includes the Kusaha reach where the August 2008 avulsion occurred.

The explanation for such variability lies in the underlying principle in these approaches. The S_{cv}/S_{dv} ratio criterion (Mackey and Bridge, 1995) emphasises the super-elevated condition of the channel, but the levee height is ignored. The L_s/S_{dv} criterion (Mohrig et al., 2000) uses the levee height and channel position, but super-elevation is not considered. Similarly, the h_e/h ratio (Bryant et al., 1995) uses channel position, super-elevation, and levee height but does not consider the down-valley slope. While all three approaches capture some bits of the processes/parameters involved in avulsion, none of these fully describe them. We have therefore attempted to integrate all three approaches and have also included planform dynamics to generate an ATI.

5.2. Planform variability and its implication on avulsion

Planform parameters such as sinuosity, braid-channel ratio, bar area, and channel area play important roles in moving the river toward avulsion threshold, particularly in a river like the Kosi that exhibits large variability in these parameters over short time scales. For example, increase in bar area is a manifestation of channel aggradation that, in turn, drives the river to a super-elevated situation. Our data (Fig. 9B) shows that the

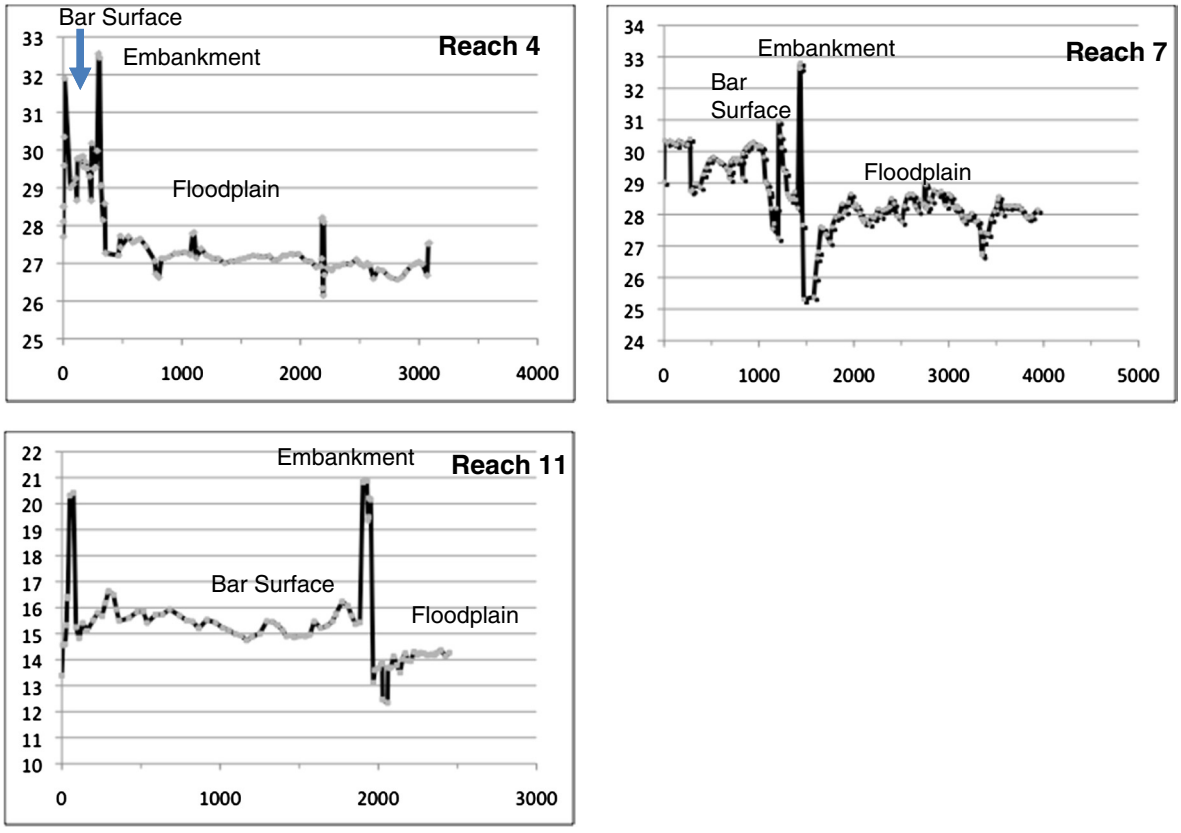

Fig. 12. Cross section profiles across reaches 4, 7, and 11 based on kinematic GPS surveys. Data from these cross sections were used to compute slope ratios for validating the SRTM-based analysis. All three cross sections show that these reaches are in super-elevated condition. Coupled with planform dynamics data, reaches 4 and 7 were classified as 'most critical', and reach 11 was designated as 'critical' for avulsion (see Fig. 11).

Table 4
Average elevation of different surfaces across eastern embankment of the Kosi River on the basis of kinematic GPS survey and computation of indices for avulsion threshold[a].

	Parameters	Reach 4	Reach 7	Reach 11
Average elevation (m)[b]	Bar	29.42 ± 0.11	29.88 ± 0.07	16.39
	Floodplain	27.1 ± 0.04	28.03 ± 0.05	13.93 ± 0.07
	Channel bed between embankments	NA	28.82 ± 0.17	15.47 ± 0.06
	Water surface (main channel)	28.84	28.26 ± 0.22	15.47 ± 0.06
	Water surface (seepage channel)	26.17	25.35	12.4
	Embankment (eastern)	32.5	32.7	20.87
Δ Elevation (m)[c]	Bar — floodplain	−2.32	−1.85	−2.46
	Channel bed between embankments — floodplain	NA	−0.79	−1.54
	Main channel — seepage channel	−2.67	−2.91	−0.99
	Bar — seepage channel	−3.25	−4.53	−3.99
Super-elevation (h_e/h)[d]	Bar — floodplain	1.75	1.66	1.55
	Channel bed between embankments — floodplain	NA	1.20	1.29
	Main channel — seepage channel	1.73	1.66	1.13
	Bar — seepage channel	2.06	2.61	1.89
Slope comparison[e]	Down-valley slope (S_{dv})		≤0.001	
	S_{cv} (bar — floodplain)	0.0087	0.0041	0.0014
	S_{cv} (bar — seepage channel)	0.0064	0.011	0.0020
	S_{cv} (channel bed between embankment — floodplain)	NA	0.0040	0.0193
	S_{cv} (channel bed between embankment — seepage channel)	NA	0.0358	0.0206
	S_{cv} (main channel — seepage channel)	NA	0.0073	0.0005

[a] Standard error was not mentioned, when datapoint over the surface are <5.
[b] Channel bed between inner and eastern embankment, which received water during flood period.
[c] Elevation difference between difference surfaces across the embankment.
[d] Super-elevation condition (h_e/h) after Bryant et al. (1995).
[e] Slope comparison after Mackey and Bridge (1995); S_{dv} — downvalley slope, S_{cv} — cross valley slope.

bar area increased in most of the reaches during the period 2000–2009, suggesting extensive aggradation during this period. Aggradation is an important process responsible for channel avulsion in a reach because it defines the superelevated condition of the channel. Significance of the aggradation process has also been reported from the Niobrara River, where aggradation in the sand-bed channel occurred because of damming in the downstream reaches (Ethridge et al., 1999). The Kosi River also exhibits extensive aggradation in several reaches (e.g., 15–18; Fig. 9B) during the period 2000–2009, but it is attributed to upstream processes (high sediment supply), flow reduction caused by the

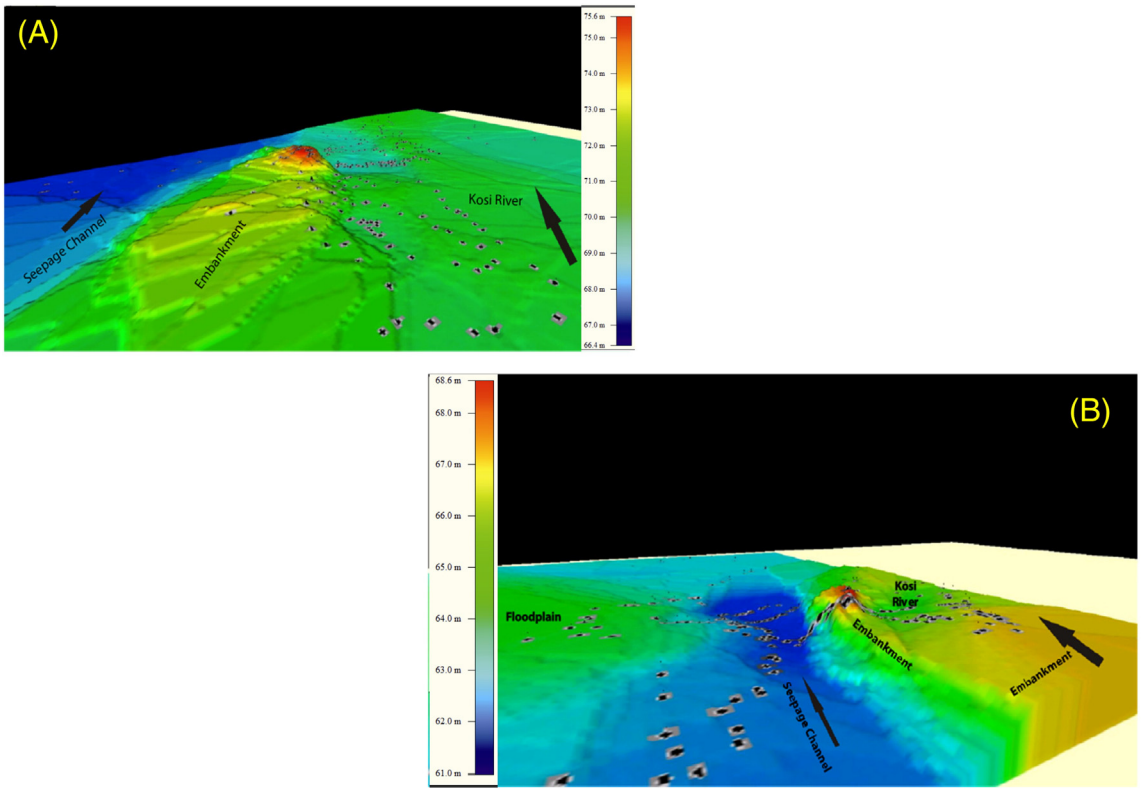

Fig. 13. Topographic mapping using the Total Station in and around the Kosi River channel around Kusaha. (A) A perspective view showing the relative positions of the Kosi River with respect to the eastern embankment and the seepage channel. (B) The Kosi River is flowing in a super-elevation condition as the bar surfaces are 2–3 m higher than the surrounding floodplain surface.

barrage, and presence of embankments on both sides. Braid-channel ratio has increased in these reaches, and this is attributed to the increase in channel multiplicity caused by aggradation.

The position of the channel with respect to the embankment also plays an important role in triggering avulsion. Our data shows that the Kosi River has been very dynamic within the embankment, and the main channel flow has been oscillating between the left and right embankments very frequently (Fig. 10). The 'superelevated' reaches where the channel is flowing very close to the embankment have a higher potential for avulsion. Fig. 10 shows that the main channel was hugging the eastern embankment in the reaches close to Kusaha since 2000, which triggered the avulsion in August 2008.

In general, increase in sinuosity variation provides a positive feedback on avulsion (Jones and Schumm, 1999). However, the sinuosity values of the Kosi River are quite low ($P = 1–1.25$) for most of the reaches, and they do not show much variability through time (Fig. 7). Therefore, we suggest that the sinuosity parameter does not have significant control on avulsion of the Kosi River.

5.3. Causes and controls of avulsion

As mentioned earlier, the August 2008 avulsion occurred at a discharge of 4320 m^3/s as against the design discharge of 28,500 m^3/s for the Kosi barrage and the embankments. Hydrological data for the Kosi River suggests that the avulsion discharge was about 40% of the bankfull discharge (7458 m^3/s) and less than half of the mean annual flood (9183 m^3/s) at Birpur (Sinha et al., 2008). The maximum observed discharge at Birpur has been recorded as 14,833 m^3/s, which is much higher than the discharge on 18 August 2008 when the avulsion occurred. Our data suggest that the August 2008 avulsion was not caused by a large flood event, and this validates the earlier suggestions that the 'normal' hydrological flows can 'trigger the avulsion if the river is close to the avulsion threshold' (Brizga and Finlayson, 1990; Ethridge et al., 1999; Jones and Schumm, 1999). The Kosi River is one of the highest sediment load carrying rivers in the Ganga basin with an annual sediment load of 43 million tonnes/year (Sinha and Friend, 1994; Sinha, 2009). Further, the ratio of upland to plains area for the Kosi River catchment is 5.3 (Sinha and Friend, 1994); this means that the available depositional area for accommodating such large sediment flux is quite small. Extensive sedimentation coupled with rapid migration in the alluvial plain has generated a large depositional landform, the Kosi megafan (120 km wide and 150 km long), over the geological period. However, the construction of embankments on both sides of the Kosi around 1955–1956 and that of the Kosi barrage at Birpur in 1963 reduced the effective depositional area dramatically and this resulted in rapid channel aggradation. Although no topographic survey data are available for the pre-barrage period, our surveys have shown that the river is presently in a super-elevated condition. We conclude that excessive channel aggradation led to the reduction of the down-valley slope (S_{dv}) and increase in S_{cv}/S_{dv} ratio. Model simulations by Mackey and Bridge (1995) used the ratio S_{cv}/S_{dv} to determine the avulsion frequency and location; our results provide a field-scale validation of the location of potential avulsion sites. Further, the presence of the Kosi barrage certainly acts as a major barrier to water and sediment flow resulting in reduction in the carrying capacity of the river, which further aggravates the sedimentation upstream of the barrage. In addition, the Kosi River channel within the 10-km-wide embankment has been laterally shifting over the years and flowing very close to the eastern embankment since 2000. It has also been eroding the spurs leading to significant seepage and toe erosion of the embankment from the inner as well as the outer side. These human-induced factors helped the breaching of the eastern embankment by the river which was already close to the avulsion threshold.

Several workers have pointed out that increase in S_{cv}/S_{dv} ratio is a necessary but not a sufficient condition for avulsion to occur (Slingerland and Smith, 2004; Aslan et al., 2005). As mentioned earlier, the Kosi River could have been close to the avulsion threshold since 2000 itself owing to 'universal' causes (Phillips, 2011) of in-channel sedimentation, but the continued planform changes, shifting of channel thalweg, development of seepage channel, and localised weakening of the eastern embankment provided the 'local' controls (Phillips, 2011). Some of these local controls are natural, but they were certainly accentuated by the human factors such as the construction of embankments and their poor maintenance.

Another important factor is the connectivity structure of the paleochannel network on the megafan surface outside the embankment. Our analysis of the connectivity structure for the pre- and post-avulsion period (Sinha et al., 2013) has shown that the 'structural' connectivity of the paleochannel network on the fan surface provided the pathway for the avulsion channel during the August 2008 event. Further, a significant flow in the seepage channel close to the eastern embankment suggests hydrological connectivity between the river and the seepage channel, in some reaches; and such sites have high potential of avulsion in near future. Sinha et al. (2013) also postulated the avulsive course of the Kosi from one of the potential sites for avulsion identified in this paper (reach 4). Therefore, the identification of such sites coupled with the connectivity model can help in delineating flood risk zones.

5.4. Implications for prediction of future avulsions

Avulsion thresholds are typically defined on the topographic variation (Bryant et al., 1995; Mackey and Bridge, 1995; Mohrig et al., 2000), which characterises the avulsion potential of any site. However, the present analysis shows that process understanding on the basis of planform dynamics can be integrated with the topographic (slope) parameters to capture the temporal variability in the parameters controlling the avulsion. The proposed avulsion threshold index (ATI) integrates the static (topographic variability) and dynamic (channel processes) components that is vital to map potential sites of avulsion. Therefore, potential (prediction) of an avulsion event may be summarised as the summation of topography-based indices, channel proximity to embankment, and channel processes on the basis of planform dynamics.

We therefore suggest that the steps to identify potential sites for future avulsions should include (i) repetitive cross section surveys to compute slope ratios, (ii) repetitive planform mapping and monitoring of thalweg position with respect to the embankment, and (iii) monitoring of discharge in seepage channels outside the embankment to assess pore pressure condition in the embankment and its vulnerability to erosion processes.

6. Conclusions

The August 2008 avulsion of the Kosi River was caused by a combination of factors such as rapid aggradation of the channel belt after the construction of an embankment, planform dynamics, and the lack of a sound monitoring mechanism. This study has provided a field-scale validation of the simulation models of avulsion proposed by earlier workers. Our proposed avulsion threshold index (ATI) combines the topography-driven factors (such as slope ratios) and process related factors (such as planform dynamics). Based on our analysis, we have identified several potential sites of future avulsions apart from the Kusaha where the August 2008 avulsion occurred. Although the Kosi River has now been restored within the embankments after the breach was plugged on 26 January 2009, several reaches including the Kusaha along the eastern embankment are still at risk as the causal factors of avulsion remain unchanged. We recommend continuous monitoring of these sites and repeated surveys of cross sections and planform as well as monitoring of the seepage channels to avoid a similar disaster in this region.

Acknowledgements

We thank the Ministry of Earth Sciences, New Delhi, for providing the financial assistance for this research through a generous grant (MOES/16/01/09/09-RDEAS). Site engineers and staff at the Kosi barrage are profusely thanked for their constant support during the execution of this research project. We are also thankful to several local organizations and NGOs that helped us in providing logistic support and hospitality during the field visits. Several students, Kumar Gaurav, Suneel Joshi, Rakesh Kumar, Rahul Kaushal, Jawed Ahmad, Vinee Srivastava, and Ashok helped during the field surveys and their help is thankfully acknowledged. We sincerely thank the reviewers for their critical comments on an earlier version of this manuscript which helped immensely to improve the paper. This is a contribution to IGCP 582 on tropical rivers.

References

Agarwal, R.P., Bhoj, R., 1992. Evolution of Kosi River fan, India: structural implication and geomorphic significance. Int. J. Remote Sens. 13 (10), 1891–1901.
Allen, J.R.L., 1965. A review of the origin and characteristics of recent alluvial sediments. Sedimentology 5 (2), 89–191.
Arogyaswamy, R.N.P., 1971. Some geological factors influencing the behaviour of the Kosi. Rec. Geol. Surv. India 96, 42–52.
Aslan, A., Autin, W.J., Blum, M.D., 2005. Causes of river avulsion: insights from the late Holocene avulsion history of the Mississippi River, U.S.A. J. Sediment. Res. 75, 648–662.
Brizga, S.O., Finlayson, B.L., 1990. Channel avulsion and river metamorphosis: the case of the Thomson River, Victoria, Australia. Earth Surf. Process. Landf. 15, 391–404.
Bryant, M., Falk, P., Paola, C., 1995. Experimental study of avulsion frequency and rate of deposition. Geology 23, 365–368.
Chakraborty, T., Kar, R., Ghosh, P., Basu, S., 2010. Kosi megafan: historical records, geomorphology and the recent avulsion of the Kosi River. Quat. Int. 227, 143–160.
Ethridge, F.G., Skelly, R.L., Bristow, C.S., 1999. Avulsion and crevassing in the sandy, braided Niobrar River: complex response to base level rise and aggradation. In: Smith, N.D., Rogers, J. (Eds.), Fluvial Sedimentology VI. Spl. Pub. International Association of Sedimentologist, 28. Blackwell Science, Oxford, UK, pp. 179–191.
Friend, P.F., Sinha, R., 1993. Braiding and meandering parameters. In: Best, J.L., Bristow, C.S. (Eds.), Braided Rivers. Geological Society of London Special Publication, 75, pp. 105–111.
Geddes, A., 1960. The alluvial morphology of the Indo-Gangetic plain: its mapping and geographical significance. Trans. Inst. Br. Geogr. Publ. 28, 253–277.
Gohain, K., Parkash, B., 1992. Morphology of the Kosi megafan. In: Rachocki, A.H., Church, M. (Eds.), Alluvial Fans: A Field Approach. John Wiley and Sons Ltd., New York, pp. 151–178.
Gole, C.V., Chitale, S.V., 1966. Inland delta building activity of Kosi River. J. Hydraul. Div. ASCE 92, 111–126.
Jain, V., Sinha, R., 2003. Hyperavulsive-anabranching Baghmati River system, north Bihar plains, eastern India. Z. Geomorphol. 47 (1), 101–116.
Jain, V., Sinha, R., 2004. Fluvial dynamics of an anabranching river system in Himalayan foreland basin, Baghmati River, north Bihar plains, India. Geomorphology 60, 147–170.
Jain, V., Tandon, S.K., Sinha, R., 2012. Application of modern geomorphic concepts for understanding the spatio-temporal complexity of the large Ganga river dispersal system. Curr. Sci. 103 (11), 1300–1319.
Jones, L.S., Schumm, S.A., 1999. Causes of avulsion: an overview. In: Smith, N.D., Rogers, J. (Eds.), Fluvial Sedimentology VI. Spl. Pub. International Association of Sedimentologist, 28. Blackwell Science, Oxford, UK, pp. 171–178.
Kale, V.S., 2011. Himalayan catastrophe that engulfed North Bihar. J. Geol. Soc. India 72, 713–719.
Karssenberg, D., Bridge, J.S., 2008. A three-dimensional numerical model of sediment transport, erosion and deposition within a network of channel belts, floodplain and hill slope: extrinsic and intrinsic controls on floodplain dynamics and alluvial architecture. Sedimentology 55, 1717–1745.
Mackey, S.D., Bridge, J.S., 1995. Three-dimensional model of alluvial stratigraphy: theory and application. J. Sediment. Res. B65 (1), 7–31.
Mishra, D.K., 2008. The Kosi and the embankment story. Econ. Polit. Wkly. 43, 47–52.
Mohrig, D., Heller, P.L., Paola, C., Lyons, W.J., 2000. Interpreting avulsion process from ancient alluvial sequences: Guadalope–Matarranya system (northern Spain) and Wasatch Formation (western Colorado). Bull. Geol. Soc. Am. 112, 1787–1803.
Phillips, J.D., 2011. Universal and local controls of avulsions in southeast Texas rivers. Geomorphology 130, 17–28.
Richards, K., Clifford, N.J., 2011. The nature of explanation in geomorphology. In: Gregory, K.J., Goudie, A.S. (Eds.), The SAGE Handbook of Geomorphology. SAGE Publications, London, pp. 36–58.
Saaty, T.L., 1980. The Analytical Hierarchy Process. McGraw-Hill, New York pp. 20–25.
Siddique, M.Z., Everett, J.W., Baxter, E.V., 1996. Landfill siting using geographic information system: a demonstration. J. Environ. Eng. ASCE 122 (6), 515–523.
Singh, R.L., 1994. India: a regional geography. National Geographical Society of IndiaUBS Publishers Distribution Limited, Varanasi, India pp. 183–252.
Sinha, R., 2009. The great avulsion of Kosi on 18 August 2008. Curr. Sci. 97 (3), 429–433.
Sinha, R., Friend, P.F., 1994. River systems and their sediment flux, Indo-Gangetic plains, northern Bihar, India. Sedimentology 41, 825–845.
Sinha, R., Bapalu, G., Singh, L., Rath, B., 2008. Flood risk analysis in the Kosi River basin, north Bihar using multi-parametric approach of analytical hierarchy process (AHP). J. Indian Soc. Remote Sens. 36 (4), 335–349.
Sinha, R., Gaurav, K., Chandra, S., Tandon, S.K., 2013. Exploring the channel connectivity structure of the August 2008 avulsion belt of the Kosi River: application to flood risk assessment. Geology 41, 1099–1102.
Slingerland, R., Smith, N.D., 1998. Necessary conditions for a meandering river avulsion. Geology 26, 435–438.
Slingerland, R., Smith, N.D., 2004. River avulsions and their deposits. Annu. Rev. Earth Planet. Sci. 32, 257–285.
Stouthamer, E., Berendsen, H.J.A., 2007. Avulsion: the relative roles of autogenic and allogenic processes. Sediment. Geol. 198, 309–325.
Törnqvist, T.E., Bridge, J.S., 2002. Spatial variation of overbank aggradation rate and its influence on avulsion frequency. Sedimentology 49, 891–905.
Wells, N.A., Dorr, J.A., 1987. Shifting of the Kosi River, northern India. Geology 15, 204–207.